



# Comparing the effect of electrode geometry on resistance spot welding of aluminum alloys between experimental results and numerical simulation

Markus Tuchtfeld<sup>1</sup> · Stefan Heilmann<sup>2</sup> · Uwe Füssel<sup>2</sup> · Sven Jüttner<sup>3</sup>

Received: 4 September 2018 / Accepted: 21 November 2018 / Published online: 5 January 2019  
© International Institute of Welding 2019

## Abstract

With the tightened emission limits the amount of aluminum sheets in future body-in-white concepts is on the rise. Thus, there is a need for optimizing the joining techniques to fulfill the upcoming challenges linked to high volume production. Especially the electrode life for resistance spot welding as a reliable and established process needs to improve. In order to do so the effect of electrode geometries on the electrode life is investigated. It is shown that the radius of curvature, the size of the face diameter, and the cone angle influences the electrode life. The reason for this behavior is explained by a numerical simulation developed by the TU Dresden. Based on these findings, an analysis with the purpose of investigating an improved electrode geometry is conducted. It is shown that a domed electrode with a radius of curvature of 150 mm should be used. This electrode combines the ability to crack the oxide layer effectively while ensuring a sufficient area of contact between electrode and sheet.

**Keywords** Aluminum alloys · Resistance spot welding · Resistance welding electrodes · Contact resistance · Simulating

## 1 Motivation

For the process-reliable and cost-effective joining of aluminum materials by resistance spot welding, the influence of contact resistance is the biggest challenge. This depends directly on the insulating natural oxide layer on the aluminum surface. The oxide layer is irregular in its composition and thickness over the entire surface and thus always requires different starting situations during welding [1]. In addition, due to the increased contact resistance, it leads to a locally limited strong heating between the electrode and the metal

sheet. Temperatures up to the softening range of the commonly used CuCr1Zr alloy are expected. In combination with the high affinity between copper and aluminum, this leads to increased electrode wear and thus constantly changing contact situations. The resulting always new initial situation with regard to the contact resistance does not allow a reproducible welding result with consistent welding parameters.

In order to use the resistance spot welding for the joining of aluminum materials in the body construction cost-effectively, the resistance of the aluminum surface must be reproducibly lowered. The use of the electrodes as the contact point between sheet metal and joining part has a significant influence on the contacting and the wear behavior in resistance spot welding. Thus, the optimization of the electrodes, with regard to aluminum welding, is a more promising possibility for a reproducible process. The different types of electrode caps are standardized according to DIN EN ISO 5821 [2]. According to Hicken, the selection of a suitable electrode geometry is based on requirements regarding the load-bearing behavior of the connection, the wear behavior, and the maximum permissible electrode indentation [3]. In the literature, for the spot welding of aluminum alloys crowned electrode caps of type A and B (see Fig. 1) as well as flat electrodes of type C are recommended. In contrast to the flat electrode caps of type

---

Recommended for publication by Commission III - Resistance Welding, Solid State Welding, and Allied Joining Process

---

✉ Markus Tuchtfeld  
markus.tuchtfeld@volkswagen.de

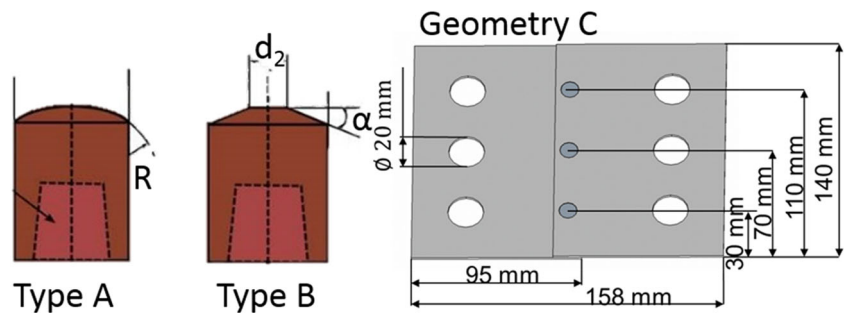
Stefan Heilmann  
stefan.heilmann@tu-dresden.de

<sup>1</sup> Volkswagen Group, Wolfsburg, Germany

<sup>2</sup> Institute of Manufacturing Technology, Chair of Joining Technology and Assembly, Technische Universität Dresden, Dresden, Germany

<sup>3</sup> Institute of Materials and Joining Technology, Otto von Guericke University Magdeburg, Magdeburg, Germany

**Fig. 1** Electrode geometries for type A and type B with a diameter of 16 mm after [2] and the multiple welding point sample geometry C



C, crowned electrodes of types A and B offer the advantage of punctiform contacting and, associated therewith, increased surface pressure. Through this, a higher current density and an improved focusing of the welding current is realized on the electrode center. Furthermore, the formation of a metallic contact during the retention period is facilitated [3–6].

Further advantages of crowned caps are the reduced splattering tendency, the reduced electrode force requirement and the possibility of compensating for low process disturbances [7]. Type B electrodes have a radius tapered contact surface. Due to their flexible design options and ease of machining, electrodes of this type represent the electrode geometry most frequently used for automotive steel construction [5]. The influence of the angle of axial taper on the electrode life is contrasted with different results. Ikeda's studies show a 50% reduction in electrode life with a 45° to 15° angle reduction [8]. The simulation results which are described by Li in [5] confirm the trend of Ikeda. According to Li, reducing the angle from 60° to 15° results in a 42% increase in electrode life. The explanation given is the improved heat removal and the lower total temperatures [5]. The results reported by Bowers in [7] show an opposite trend. Based on a simulation, a homogenization of the current density distribution in the electrode caps is detected, resulting in an increased electrode life and a reduced welding power requirement [7].

The size with which the radius of curvature is carried out in caps of types A and B is a controversially discussed topic in the literature. While in [9] is merely noted that the radius of curvature should not be too low due to the necessary heat dissipation, there are concrete recommendations in other sources. These are diverse and lie between 40 mm from Ostermann and up to 150 mm from Eichhorn [3, 10–12]. Sigler opposes a large radius, because with low radii, the current input into the material, and thus, the process reliability is improved [13].

Although, according to Browne, flat electrodes of type C reduce the electrode penetration depth, the disadvantages of the increased welding current requirements and the tendency to form a ring weld [14] prevail.

One way to increase the electrode life and process reliability is a surface profiling of the electrode caps. With the help of geometric figures generated in the electrode surface, the

formation of metallic initial contacts is facilitated by an improved breaking of the oxide layer. The resulting reduced heat generation and the homogenization of the current density caused in this way an increased electrode life. By using a milled groove profile, Kunze reports a doubling of the tool life and an increased welding area [15]. Carlson confirms the increased electrode life and additionally describes profile-induced improvements in process robustness [16]. A new approach for the structuring of electrodes is given by Heilmann [17]. By using the direct laser interference patterning micrometer-scale structures are created that reduce contact resistance by more than 50%.

Common welding electrode diameters for spot welding of aluminum are 16 mm and 20 mm. Kunze's comparative studies show a 3.5 kA larger welding current range when using 20-mm-diameter electrode caps. The reason can be found in the lower thermal load due to a higher heat capacity for the larger electrode [15]. In [18], it is further noted that due to the increased diameter of the caps, higher electrode forces can be used in welding. This positively influences the contact resistance and homogenizes the current density so that a lower tendency to thermal alloying is the result [18].

Based on the state of the art shown in the literature, the influence of crowning, the tip face, and the cone angle on the welding result during resistance spot welding of an aluminum alloy is intended to be shown in this work.

## 2 Experimental study

### 2.1 Materials and welding equipment

The aluminum alloy EN-AW-6016, which is common for European automotive applications, is used to conduct the welding experiments. The thickness of each sheet is 1.5 mm, and the surface condition is coil-passivated with lubrication. The heat treatment condition is T4. Detailed specification of the used material is given in Table 1.

For the welding experiments, two specimen geometries are used. For every investigation where it is necessary to determine the weld nugget diameter, sample geometry A is used. It is a single point welding specimen with dimensions

**Table 1** Mechanical properties and chemical composition of the 6016-T4 aluminum alloy

Tensile strength in MPa	Yield strength in MPa	Alloying elements in wt.%						
		Si	Fe	Cu	Mn	Mg	Cr	Ti
219	106	1.07	0.24	0.1	0.15	0.35	0.01	0.01

of 50 mm × 50 mm. This geometry ensures enough distance to the edges in order to avoid current shunting effects which can be significant for the resistance spot welding of aluminum [12, 19]. Sample geometry B is used for the determination of the lap shear strength. The dimensions for the sample are based on the standard DIN EN ISO 14273 [20] with the overlap shortened from 35 to 18 mm to provide a realistic comparison for actual body-in-white flanges. Geometry C is a welding sample for the determination of the tensile strength of multiple welding spots (see Fig. 1). The purpose of a multiple spot geometry is to investigate if there is a correlation between an increase of the joining gap and a decrease of the strength properties. The dimension of a single specimen is 140 mm × 95 mm. Two specimens are welded together with three welding spots distributed on an 18 mm overlap. The welds are conducted using a servo-motoric welding gun designed for the special demands of aluminum welds with the ability to provide high electrode forces up to 8 kN and welding current up to 55 kA. To endure the high forces, the arm of the C-frame is strengthened at this welding gun. The flow volume of the welding gun coolant is regulated to 8 l/min to provide constant welding conditions. For this study, a single impulse current profile is used. The electrode force, squeeze, and forge times as well as the downslope time are given in Table 2.

## 2.2 Welding electrodes

Within all tests, electrode caps made of copper-chromium-zirconium (CuCr1Zr) with 16-mm diameter are used. The use of 16 mm caps is necessary to fulfill the challenging flange range diameters required for the future use in automotive high volume production. The investigation of the correlation between electrode cap geometry and electrode cap wear is based on a variation of the geometric characteristics shown schematically in Fig. 1. The influence of the radius of curvature is explored on the basis of the prior art using five different degrees of radii. The investigation of the relationship between the diameter of the tip face and the electrode

**Table 2** Constant resistance spot welding parameters

Electrode force	Squeeze time	Welding time	Downslope	Forge time
5 kN	250 ms	60 ms	400 ms	250 ms

life is carried out on the basis of the maximum permissible electrode indentation with a minimum tip face diameter of 12 mm. The variation of the point angle is carried out in consultation with the milling system manufacturer within the technically reasonable limits of 36° or 65°. The geometry properties of the electrode caps used are described in Table 3.

## 2.3 Determination of the welding current range

While the determination of suitable welding parameters in the resistance spot welding of steel materials is usually carried out in the form of a welding range diagram, a transferability of this procedure to aluminum materials is not suitable. In particular, the upper welding range limit, which is characterized by the occurrence of weld splatter according to DIN EN ISO 14327 [21], cannot be achieved with the combination of electrode cap geometry, sheet material, electrode force, and system technology used in this work. Furthermore, due to the resulting minimum electrode life, a weld parameterization oriented at the splatter border would not have any significance for industrial applicability. Instead of the welding range diagrams, the growth curves from the determination of the nominal welding current intensity are therefore used for this work. In these, after a welding process with a low welding current, the change in the spot diameter is determined as a function of the welding current used at a constant electrode force. As the current step width, the welding current is increased based on a minimum current in increments of 1 kA up to a maximum current. The minimum current is reached at a minimum spot diameter of  $d_{pmin} = 4 \cdot \sqrt{t}$ . The maximum current is defined as the current at which the nominal spot diameter of  $d_{penn} = 5 \cdot \sqrt{t}$  is exceeded by 15%. On the basis of the diagrams determined in this way, a qualitative comparison of the influence of different process variables and process modifications on welding current and nugget size is possible.

Table 4 shows the parameters used for the preconditioning of the electrodes before the determination of welding current range.

**Table 3** Characteristics for electrode geometries of type A and type B

Radius of curvature R in mm	25	80	150	200	300
Tip face diameter $d_2$ in mm	12/16	12/16	12/16	16	16
Cone angle $\alpha$ in °	56	36/65	36		

**Table 4** Parameter for preconditioning of electrodes

Quantity	Welding current	Welding time	Downslope
5	25 kA	60 ms	0 ms

## 2.4 Wear tests

Although the inconsistent evaluation resulting from the multitude of possible quality characteristics between different publications is already criticized previously, until today there is no uniform standard of evaluation [6].

In this work, the criterion for sticking of the electrode to the sheet material, which is recommended in the literature, is used as the end of electrode life [22, 23]. The tests carried out in [24] shows that the sticking of the electrode to the sheet material is the criterion that meets the highest quality requirements. The early cancellation prevents both a reduction in surface quality and a reduction in corrosion resistance due to significant intermetallic phase formation [15]. Rashid describes in [23] the sticking of the electrodes as a criterion, which has a reproducible, clearly defined endpoint and thus seems suitable for a comparison of the electrode life. In this work, the electrode is considered worn if a firm connection between the electrode and the surface of the sheet is recorded either visually or audibly. For a uniform comparability of the different examination focuses, the comparison nugget diameter of  $d_{pver} = 1.15 \cdot 5 \cdot \sqrt{t}$  welded with the maximum current is used in all investigations. This selection of the maximum current is assumed from the automotive industry and also maps the “worst case scenario” for the achievable electrode life. After a change of the welding parameters or between the different series the electrodes are cleaned and reshaped with a tip dresser.

## 2.5 Thermography

The measurement of the temperatures during the welding process is conducted by an ImageIR8300 thermographic camera system. Because of several physical differences between aluminum and steel, it is not possible to use the established cross section model which is introduced in [25]. Instead, the camera is mounted in front of the welding gun with the specimen in the center of the frame as shown in Fig. 2. With this setup, it is

**Fig. 2** Setup for temperature determination while welding



possible to measure the temperature on the outer surface of the electrode caps which can be taken as an indication for the energetic losses during the welding process. The edges of the specimens and the front of the electrode caps are coated with graphite lacquer to minimize reflections and to ensure a defined emissivity.

## 3 Simulative analysis

The analysis of the resistance spot welding process using FEM was done with the workbench of ANSYS® Academic Associate Mechanical, Release 18.1. The investigations for the welding of aluminum alloys were carried out with the further developed model from Heilmann [26]. The goal is to better understand and explain the influence of electrode geometries on wear behavior.

Temperature-dependent mechanical, thermal, and electrical material data were determined for the Multiphysics simulation (Tables 5, 6, 7, and 8).

The plastic deformation is considered by using the flow curves of an EN-AW-6022 alloy in the T6 state and the CuCr1Zr alloy from the publication by Wan et al. [27].

For the simulation, the enthalpy  $H$  is calculated using Eq. 1.

$$H(T) = \int_{T_0}^T \rho(T) * C(T) dT \quad (1)$$

As can be seen in Table 5 and Table 7, the temperature-dependent specific resistance  $\rho$  and the heat capacity  $C$  in own measurements were determined only up to the melting temperature. The change in enthalpy during melting was determined from the data of Wang et al. [28].

The geometry modeling of the simulation model is carried out analogously to the electrode geometries shown in Table 3 with the DesignModeler. The utilization of the rotational symmetry of the resistance spot welding process enables the reduction of a 3D geometry into a 2D model (see Fig. 3).

The discretization of the geometry into finite elements took place in the contact areas with a maximum size of 0.2 mm. The element size of the remaining geometry is coarser with a maximum size of 0.375 mm. Also, the mesh has no midside nodes. Since the ANSYS Workbench has no analysis systems to do a Multiphysical simulation, the simulation is done by the usage of a transient structural system. To get a Multiphysical

**Table 5** Thermal and electrical material properties for EN-AW-6016 (sheet material)

Temperature (°C)	20	200	300	500	570
Specific resistivity ( $\Omega\text{m}$ )	3.4E-08	5.19E-08	6.33E-08	9.1E-08	1.079E-07
Thermal conductivity (W/m K)	158	163	163	154	183
Heat capacity (J/g K)	0.886	0.936	0.947	1.018	1.042
Density ( $\text{g}/\text{cm}^3$ )	2.696	2.662	2.64	2.594	2.576
Thermal expansion coefficient (ppm/K)	–	23.46	24.96	26.91	27.9

simulation in ANSYS Workbench the element “Plane223” was implemented with the APDL command “et,matid,plane223,111” for every generated geometry part. To get axisymmetric simulation again, afterwards the keyoption 3 of the element has to be changed by using the command “keyopt,matid,3,1.”

The contact areas, which are marked in Fig. 3 with the numbers 1, 2, and 3, are constructed with the contact elements “Conta172” and “Targe169.” Since these elements are automatically chosen by the transient structural analysis system, only the used degrees of freedoms have to be changed by the APDL command “KEYOPT,cid,1,3.”

Other settings, such as the frictional contact with a coefficient of 0.2 and the use of the augmented Lagrange method with an aggressive update of the stiffness at each iteration, can be done directly in the GUI of the Workbench. As boundary conditions (comparison Fig. 3) for the simulation of the resistance spot welding process, the heat transfer coefficients for the heat convection were assumed to be  $70 \text{ W}/(\text{m}^2 \text{ K})$  and implemented by the APDL command “SF,all,CONV,70,20.” Also a fixed temperature of  $20 \text{ °C}$  for the water cooling at the electrodes was implemented by the command “D,all,Temp,20,0.” The voltage and displacement in the Z direction were each set to zero at the bottom of the lower electrode. Since the Workbench provides the commands for the structural boundary conditions for the analysis system used via the GUI, only the voltage must be specified as a constraint via the command “D,all,VOLT,0.”

The welding current and the electrode force are applied via the upper side of the upper electrode. As with the displacement, the force can be specified as a boundary condition via the Workbench GUI. The welding current can only be applied to on node, that is why all nodes on the line which define the upper side of the electrode have to be coupled by the

**Table 6** Mechanical material properties for EN-AW-6016 (sheet material)

Temperature (°C)	20	100	200	400	500
Young’s modulus (GPa)	72.63	69.21	64.8	56.57	53.64
Shear modulus (GPa)	26.82	25.79	24.22	21.27	20.27
Poisson’s ratio	0.35	0.33	0.35	0.21	0.23

command “cp,1,volt,all.” Of the coupled nodes, the node with the smallest number is selected via the command “\*get,n1,node,num,min” and a predefined table of the current and time is implemented over “f,n1,amps,%current%.”

The force profile or current profile used for the simulation was adapted to the tests carried out.

To calculate the heat generated at the contact surfaces, ANSYS requires the electrical contact conductivity (ECC). For the heat transfer in contact, the thermal contact conductivity TCC is used.

The ECC (Eq. 2) is the reciprocal of the electrical contact resistance (ECR).

$$ECC = \frac{1}{ECR} \quad (2)$$

The calculation of the TCC (Eq. 3) takes place via the ECC, the Lorentz constant  $L$ , and the absolute temperature  $T$ .

$$TCC = ECC \cdot L \cdot T \quad (3)$$

For the calculation of the ECR, different formulas can be used from the literature [29].

In this work, the ECR calculation (Eq. 4) which was introduced by SORPAS is used [29, 30].

$$ECR(T, P) = 3d \left( \frac{\rho_1(T) + \rho_2(T)}{2} \right) \left( \frac{\sigma_{YS}(T)}{P} \right) \quad (4)$$

The calculation takes place by varying the pressure  $P$  and the temperature  $T$  by means of the specific material resistances of the contact partners  $\rho_1$  and  $\rho_2$  and the yield strength of the softer material  $\sigma_{YS}$ . Furthermore, the thickness of the contact layer  $d$  has an influence on the resistance. In this work, the typical value of  $0.05 \text{ mm}$  for  $d$  is assumed [27, 30].

The ECR values are crucial for the development of heat in the contact zones and thus also for the formation of the weld nugget. The equation for calculating the contact resistance according to SORPAS (Eq. 4) is described in the publication by Hamedi et al. [29] as comfortable but not well verified. This was reflected in the first simulation results again. The simulated weld nuggets were about  $2 \text{ mm}$ . For this reason, an adjustment factor  $\zeta$  has been added in Eq. 5, to calibrate the values of Eq. 4.



**Table 7** Thermal and electrical material properties CuCr1Zr (electrode material)

Temperature (°C)	18	200	300	500	700	900
Specific resistivity (Ωm)	2.11E-08	3.25E-08	3.87E-08	5.43E-08	6.99E-08	9.81E-08
Thermal conductivity (W/m K)	326	305	291	281	310	268
Heat capacity (J/g K)	0.39	0.393	0.395	0.4	0.482	0.494
Density (g/cm <sup>3</sup> )	8.882	8.803	8.755	8.656	8.549	8.425
Thermal expansion coefficient (ppm/K)	–	16.51	17.19	18.01	18.86	20.19

$$ECR(T, P) = 3d \left( \frac{\rho_1(T) + \rho_2(T)}{2} \right) \left( \frac{\sigma_{YS}(T)}{P} \right) * \zeta \quad (5)$$

The factor was adjusted using the experiments of the electrode geometry R150AF16 so that at a current of 41 kA a nugget diameter of about 7 mm is determined. This factor was subsequently used for the simulation of all electrode geometries. The ECC and TCC values have to be applied in the Workbench by changing the real constants of the contact elements (cid). For this, the predefined tables have to be implemented with the command “rmodif,cid,14,%TCC\_AI\_AI%” for the TCC values and “rmodif,cid,19,%ECC\_AI\_AI%” for the ECC values. To define the temperature where the contact has to change from frictional to bonded because of melting, the command “rmodif,cid,35,660” should be implemented. If a symmetric contact behavior is chosen in the Workbench, every modification of the real constant should be also done with the target elements (tid).

## 4 Investigation of the electrode cap radius

### 4.1 Influence of the electrode cap radius on the nugget growth

The use of different electrode radii significantly influences the welding process, so that the geometry-dependent welding growth curves are determined to ensure constant process conditions (see [13]). Based on Fig. 4, an inverse correlation between an increase in the electrode cap radius and the spot diameter at discrete weld currents is detected.

The nominal nugget diameter required for the connection is exceeded depending on the electrode cap radius with welding currents between 37 and 42 kA. The nugget diameter, which is welded with an electrode cap radius of 25 mm compared to an

**Table 8** Mechanical material properties CuCr1Zr (electrode material)

Temperature (°C)	20	200	400	600	800	900
Young’s modulus (GPa)	87.82	81.04	76.97	69.61	65.11	60.59
Shear modulus (GPa)	33.08	31.19	30.12	28.29	26.33	25.03
Poisson’s ratio	0.33	0.3	0.27	0.31	0.33	0.34

electrode cap radius of 300 mm for a welding current of 40 kA, is increased by 28%. To explain these differences, the welding process simulation is used based on three exemplary electrode cap radii. The determination of the current density as well as the temperatures is carried out directly in the joining plane, so that a geometry-unaffected evaluation of the process variables takes place. By increasing the crowning correlated increase in the contact area between the electrode cap and sheet, the current density decreases in the joining plane. This can be clarified on the basis of the simulation. Figure 5 shows the temperature and the current density at the time of the maximum current in the joining plane. In addition, the contact zone between the sheets is illustrated by the green vertical lines.

The changed current conductor cross section results in a reduced heat generation in the joining plane, for caps with greater crowning. Thus, a correlation between reduced electrode cap radius and temperature is apparent. The simulation (Fig. 5) shows that the temperature increase in the joining plane takes place slower for electrodes with greater crowning. Furthermore, different maximum temperature can be seen. While maximum temperatures of 956 °C are present for the 300-electrode cap, the electrode caps of 25-radius reach up to 986 °C. The determination of the total energy required to form

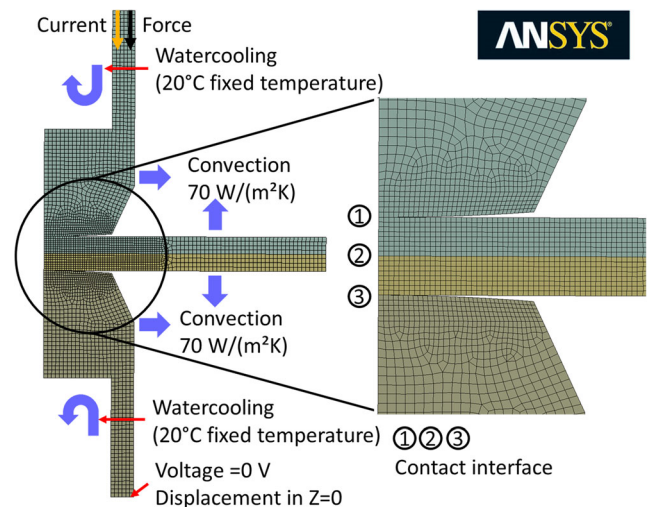


**Fig. 3** Model structure of the FEM simulation, showing the boundary conditions, mesh and contact interfaces on the example of the R80AF12-65 electrode

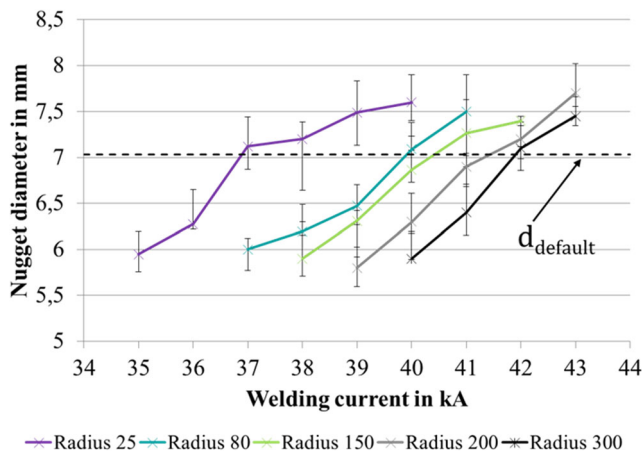


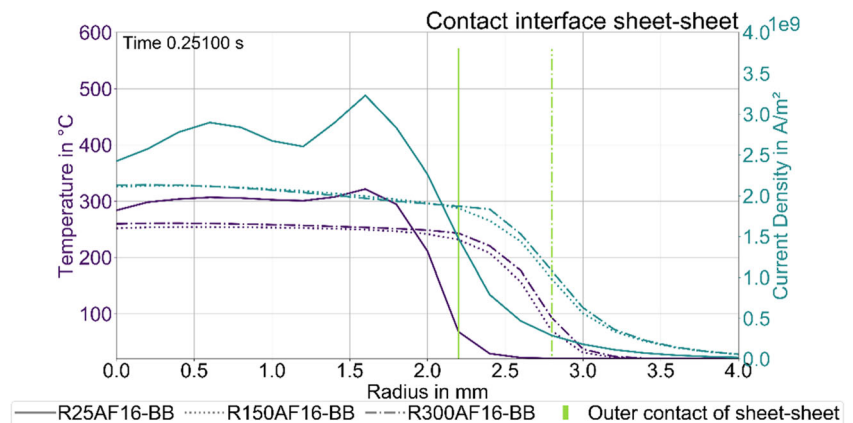
Fig. 4 Nugget growth curve with variation of electrode cap radius as a result out of experimental examinations

the nominal diameter shows a difference between radius 25 and radius 300 of 14.46%.

### 4.2 Influence of the electrode cap radius on the electrode indentation and joining gap

Depending on the electrode radius, the welded samples show optical differences in surface appearance. Table 9 shows the indentation depths and joining gap determined on the basis of five welding samples in each case. As can be seen from the table, both the electrode indentation depth and the joining gap increase with decreasing electrode cap radius. In particular, the samples welded with the radius 25 have a comparatively strong electrode indentation, which corresponds to about 30% of the original sheet thickness. It is noticeable that even with a radius of 80 the electrode indentation depth decreases significantly and approaches a nearly constant value of less than 8% of the original sheet thickness from the radius of 150. Analogous to this, no significant differences in the gap formation are detected from a radius of 80 onwards. An explanation for this behavior is the contact situation between the electrode and the sheets. A reduction of the electrode cap radius results

Fig. 5 Comparison of the simulated temperature and current density in the joining zone for electrode cap radius 25, 150, and 300 mm at the end of the current upslope



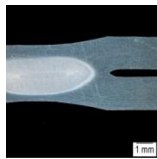
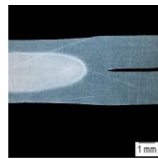
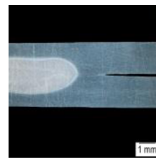
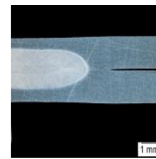
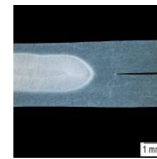
in an increase of the local pressure from electrode to material surface. A lower resistance to the sinking of the electrode in the material is the result. The area of the electrode indentation shown in Table 9 clearly shows that this effect is intensified at very low radii. Due to the dome-shaped form of the electrode contact surface, however, even minor changes in the radius are sufficient to significantly increase the surface area and thus make it difficult to sink in. The observed joining gap is due to the comparatively high local plastic deformation caused by the strong sinking. The resulting tensile stresses lead to a subsequent flow of the material and thus to a gap opening. An evaluation of the welding result based on the optical properties of the electrode indentation is not made at this point due to the contrary research objective. However, with regard to further application in the automotive field of vision, pronounced electrode indentation can result in a negative weld rating.

### 4.3 Influence of the electrode cap radius on the strength properties

To exclude a possible influence on the load-bearing properties from the divergent geometrical notches resulting from spot welding with different electrode cap radii, load bearing capacity studies are carried out [6, 11, 31].

Neither single nor multipoint samples show significant differences in quasi-static tensile strength. A two-sample  $t_{test}$  for independent samples from the three-point samples gives a test value of  $t_{test} = -0.447$  for comparison between the lowest and highest radii. Based on this, it can be stated that with a confidence of 95% there are no radius-dependent differences in the maximum tensile strengths. While the tensile strength of three-point multipoint samples is 12.28 kN on average, the one-point samples have a maximum tensile strength of 3.68 kN on average. The relative increased strength of the individual points determined in a comparison of the three-point samples compared to single-point samples results from the increased sample rigidity. As a result of this, the peeling tensile component occurring in the quasi-static shear tensile test decreases, so that higher strengths are achieved.

**Table 9** Mean characteristic values of spot welds determined by the cross section evaluation

Radius R in mm	25	80	150	200	300
<b>Visualization</b>					
<b>Electrode indentation in mm</b>	0.46	0.18	0.11	0.1	0.09
<b>Joining gap in mm</b>	0.38	0.1	0.1	0.1	0.1
<b>Area - electrode indentation in mm<sup>2</sup></b>	65.26	71.63	78.57	82.15	87.33

#### 4.4 Influence of the electrode cap radius on the heat generation

The temperature measurement of the maximum temperatures on the electrode cap surfaces shows significant differences depending on the electrode radius. As shown in Fig. 6, there is an apparent relationship between a decrease in the electrode cap radius and a decrease in the cap maximum temperature based on the thermographic measurements. The highest temperatures are detected at 223 °C on the outside of the radius 150 electrode caps. By contrast, the maximum temperatures measured at radius 25 are reduced by 19 °C. The comparison with the simulation has a similar curve progression. The temperatures rise at the same speed as the measurements. At the apex, they have a maximum difference of 22 °C for the 300 mm radius electrode. The cooling rate after the current flow is faster for all simulations than for the measurements. These differences are related to the heating of cooling water and air during resistance spot welding. The resulting reduction in heat dissipation was not included in the simulation. Taking this into account, the simulation can be considered a valid illustration of reality.

These results are not readily explainable in the context of previous findings. A lower cap temperature should also have

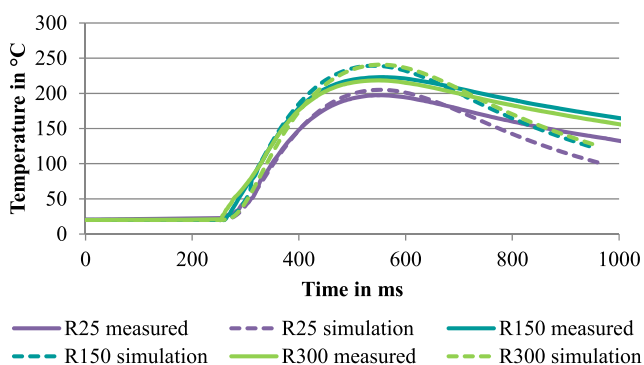


**Fig. 6** Comparison of temperature at the electrode surface for measurements and simulation

less wear. The apparent contradiction between the measured temperature curves on the outside of the cap and the electrode wear can be resolved on the basis of the extended simulation consideration of the temperature distribution over the electrode cap radius shown in Fig. 7. The temperature curve of the electrode cap of radius 25 intersects the temperature curves of the larger electrode radii in an area around the outer contacting area. In addition, a significant change in the slope of the temperature curve can be observed in the respective contact edge regions. A determination of the temperature difference between the cap center and the electrode cap jacket results in 530 °C for the electrode with radius 25. The differences of the electrode cap with radius 150 and radius 300, however, are 15% lower at about 455 °C. Viewed over the entire welding time, the maximum temperatures at the center of the caps are observed with up to 610 °C when using the radius 25 electrode. The temperature of the 300 radius electrode cap is about 10% lower at 550 °C. It is noticeable that the maximum temperatures of the cap with radius 150 are only 10 °C higher than those of the electrode cap with radius 300 which indicates an almost identical heat generation. The radius of the surface in contact increases due to the sinking of the electrode into the material for the radius 25 electrodes from 1.8 mm at the start of welding to 4.2 mm after the welding end.

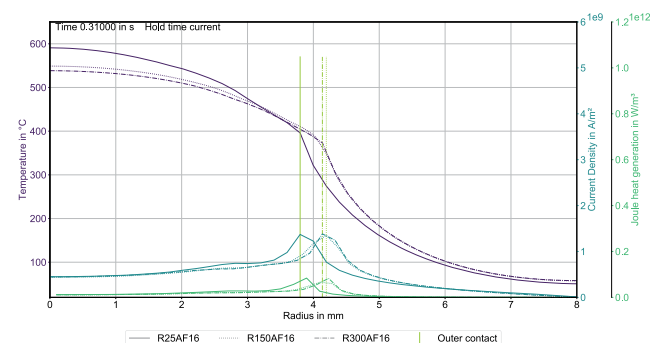


**Fig. 7** Comparison of the simulated temperature, current density, and contact pressure in the contact zone electrode-sheet for electrode cap radius 25, 150, and 300 mm at the end of the hold time of current



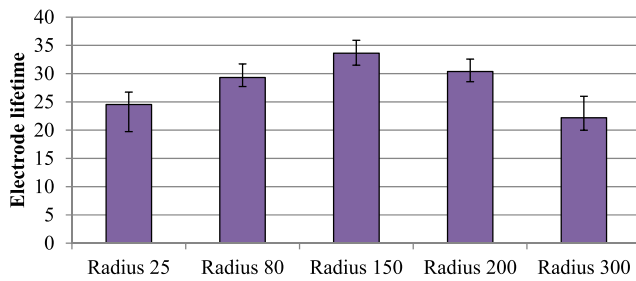


**Fig. 8** Electrode lifetime with variation of electrode cap radius

For radius 300, the radius is increased from 2.8 to 5.1 mm. The radius of contact for electrode caps with radius 150 is between 2.95 and 4.9 mm.

The explanation for the differences between the temperature in the inner and outer regions of the electrode is the position of the heat generation resulting from the geometry-dependent pressure distribution. Due to the increased contact area between the material and the electrode cap, the range of the maximum pressure distribution for the electrode caps with radius 150 and 300 is closer to the electrode shell surface compared to the cap with radius 25. Due to the increased current density caused by the lower contact resistances, this area also generates the largest amount of Joule heat. As a result of the geometry-independent multiaxial heat conduction, higher temperatures for larger electrode cap radii are to be detected in the cap outer regions due to the closer formation of heat. The simulated higher cap internal temperatures of the radius 25 electrode caps are due to the lower current passage area, which is reduced despite the increased electrode sinking (see Table 9) compared to the larger electrode radii. The increase by about 20% compared to the larger electrode caps due to the current density results in the increased Joule heat generation. Noticeable are the small temperature difference between the electrode caps with radius 150 and electrode caps with radius 300 as well as the radius of contact reduced for the radius 150. As shown by the simulation and the measurements

in Table 9, the electrode force is not sufficient for significant penetration of the radius 300 electrode caps into the sheet surface. Due to the reduced radius, the electrode caps with radius 150 sink more strongly into the material so that a larger proportion of the electrode cap surface is in direct contact. Associated with the dome-shaped expression of the electrode indentation, therefore, a significant increase in the contact surface is to be assumed despite the same contact radius of the electrode cap with radius 150 compared to radius 300. This assumption is confirmed by the analysis of the pressure distribution over the welding time. While there are pronounced pressure maxima in the center of the cap and in the contacting region in the case of the electrode cap with radius 150, the pressure distribution for the cap with radius 300 is comparatively homogeneous outside the contacting regions (see Fig. 9). Further explanations are described in the following chapter.

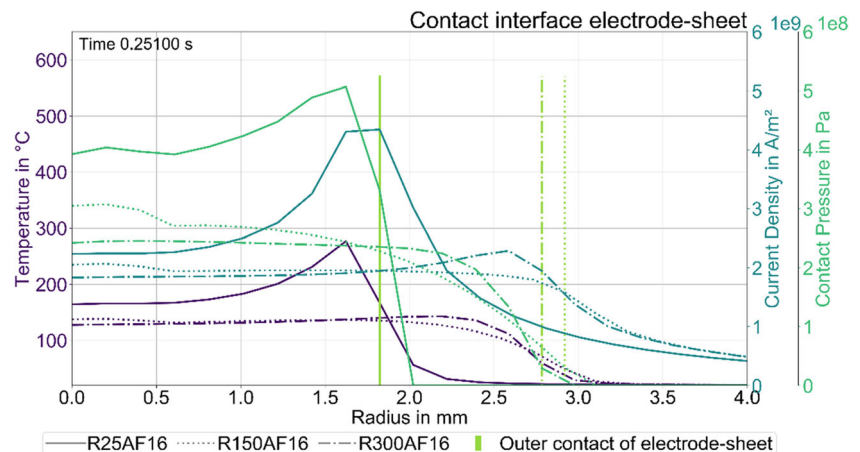
#### 4.5 Influence of the electrode cap radius on electrode lifetime

Based on the electrode lifetime shown in Fig. 8, a significant influence of the electrode cap radius on the lifetime can be seen. The lowest levels are achieved on average with 22 points with the 300 electrode cap radius. This is followed by the 25 mm caps with 24 spot welds, the 80 mm radius electrode caps with 29 points, and the 200er electrode caps with 30 points. The best results were obtained by the use of 150 mm radius electrode caps.

As an explanation for the wear behavior two opposing factors are to be considered, which can be justified by the simulation. By way of example, Fig. 9 shows the temperature, the current density, and the contact pressure in the electrode-sheet contact zone for the electrode radii R25, R150, and R300 at the end of the current upslope.

Although a reduced electrode cap radius for forming an equivalent nugget requires less welding current due to the

**Fig. 9** Comparison of the simulated temperature, current density, and contact pressure in the contact zone electrode-sheet for electrode cap radius 25, 150, and 300 mm at the end of the current upslope



increased current density, the reduced contact area results in an increased temperature in the contact area between the electrode and the sheet. It can be seen from Fig. 9 that in the case of the electrode cap with radius 25, current density peaks occur at the edge of the contact electrode and metal sheet. This can be explained by the pressure profile also shown. The current selects the path of least resistance. As the electrical contact resistance decreases with increasing pressure, the passage of current will concentrate at the edges. This results in an increased temperature development at the beginning of the welding process. The accelerated diffusion processes and the increased peak temperatures increase the wear tendency of the electrode cap and lead to premature failure. Although the comparatively large radius electrode caps have a reduced electrode cap temperature, they cannot exploit their full potential due to the electrode force which is limited because of the 16-mm electrode diameter. The homogeneous pressure distributions resulting from the low plastic deformation lead to wear-promoting current density ratios, especially in the wear-critical contact edge areas. Despite virtually the same current passage area, the electrode caps with a radius of 300 mm show an increased current density at the outer contact in comparison to the electrode cap with a radius of 150 mm. This can be explained by the distribution of the contact pressure. For radius 150, there is an increased pressure in the region of the axis of symmetry, resulting in a reduced electrical contact resistance in the region. This means favoring the passage of electricity at this point. On the other hand, there is the increased resistance of the material, which the current experiences as a result of the further travel, in order to achieve a passage with less contact resistance. These two mechanisms appear to be balanced on the 150 radius electrode cap, allowing for homogeneous current density distribution and decreasing cap wear. For the electrode cap with radius 300, a homogeneous profile of the contact pressure is shown. Thus, the contact resistance is the same over the entire area and the current passage at the outer edge of the electrode is connected to the lowest total resistance. This results in an increased current density (Fig. 9). In addition, it should be noted that in spite of nearly the same current passage area between electrode caps of radius 300 and radius 150 to form an equivalent nugget, a welding current increased by 1.5 kA is necessary (compare Sect. 4.1). The additional energy introduced in this way additionally amplifies the tendency to wear as heat loss. The difference between the electrode life of radius 25 and radius 300 can additionally be attributed to the reduced surface pressure. It can be assumed that the mechanism of contacting metal to metal is made more difficult. The reduced number of contact bridges could account for an additional proportion of electrode cap wear. In the simulation, an ideal contact is assumed. Compared to the simulation, in reality, an amplification of the described mechanisms in the area of the contact bridges can be expected.

In summary, it can be said that for a wear-optimized welding process, the choice of the radius of the electrode cap must be made as a compromise between the current transition surface and current density focusing. As cap radius, a radius of 150 is to be preferred, as this combines both requirements with each other and thus achieves the highest possible electrode life.

## 5 Investigation of the electrode tip face diameter

### 5.1 Influence of the electrode tip face diameter on the nugget growth

To investigate the influence of an electrode tip face on the nugget growth, tip faces with a diameter of 12 mm and a cone angle of  $36^\circ$  are applied. Figure 10 compares the growth curves of electrodes with and without tip face. As can be seen from the figure, electrodes with applied tip face require less power to reach equivalent nugget diameters compared to electrode caps without. The possible current reduction for the design of the nominal point diameter depends on the electrode cap radius and is 0.5 kA for the electrode caps with radius 25, 1.5 kA for the radius 80, and 2 kA for the radius 150. The comparison of the nugget diameter based on discrete welding currents shows on average an increase of 0.6 mm for electrode caps with tip face. One explanation for the differences in the growth curves is the increase in the current density resulting from the application of a tip face. Thus, the analysis of the welding simulation after reaching the maximum welding current for the electrode cap with tip face shows an 8.2% increase

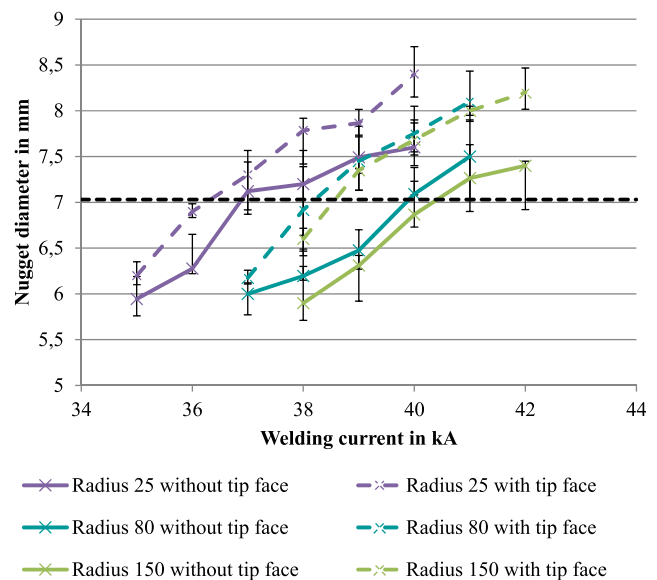
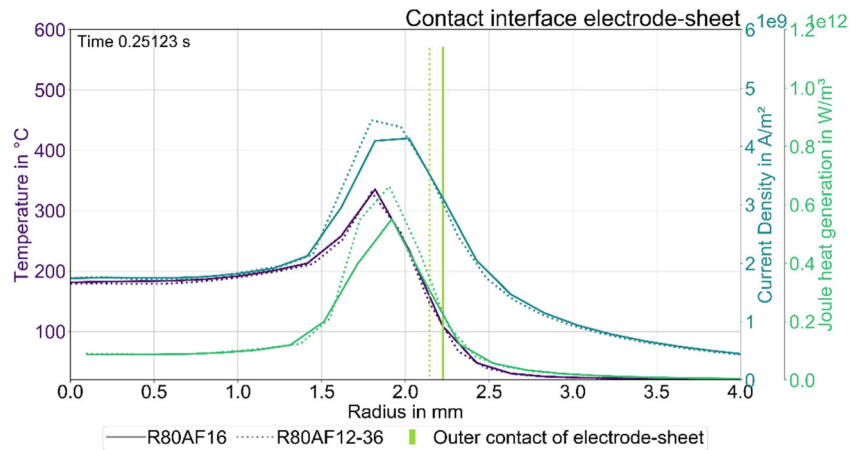


**Fig. 10** Comparison of nugget growth curve with variation of electrode cap radius and tip face

**Fig. 11** Comparison of the simulated temperature, current density, and Joule heat generation in the contact zone electrode-sheet for electrode cap radius 80 with tip face of 16 mm and 12 mm the begin of the hold time of current



in the current density in the contact plane between the cap and the sheet. To determine the reasons for the change in the current density function, the analysis and comparison of the cap indentation in the material is necessary. By measuring the cross sections, it can be seen that the application of a tip face has no effect on cap indentation and joining gap. The reason for this is the non-full-surface contact as well as the only partial sinking of the electrode cap into the sheet surface. As already shown in the previous chapter based on the simulation results, the maximum outer contact area determined with 5.1 mm is smaller than the tip face diameter used in these experiments. The light microscopic measurement of the surface indentation shows identical diameters for both the electrodes with and without tip face and thus confirms the predictions of the simulation results. With regard to the growth curves, therefore, a change in the current densities induced from the reduction of the current transfer area can be excluded. As an alternative explanatory approach, the change in the current density distribution due to the contact surface rejuvenation as shown in [5]. This results in a geometry-dependent change and focusing of the current flow lines, whereby the current density increases, in particular in the outer contacting areas. Therefore, despite the identical contact surface, the use of an electrode with a tip face also results in a greater amount of heat in the joint plane, so that a formation of a weld nugget can already take place at lower current intensities. Analogous

to this explanation, the radius-dependent differences between the electrode caps with and without tip face are to be regarded. Due to the homogenization of the current density over the electrode cap surface (see Sect. 4.5) the local effect of current density focusing on individual regions for large radii is relatively strong. A further discussion of the dependence between cone angle and current density distribution is given in Sect. 6.

### 5.2 Influence of the electrode tip face diameter on the strength and heat generation

Due to identical surface indentation as well as the independence of the load-bearing capacity from the geometric properties shown in Sect. 4.3 a discussion of the influence of an electrode tip face on the load-bearing properties of the welded joint is not necessary. The evaluation of the thermographic images of the electrode cap outside also shows no significant differences between the electrode caps with and without tip face. The results of the simulative comparison of Joule heat generation at the start of welding in the outer contact region are shown in Fig. 11. The analysis of the simulation shows for the electrode caps with applied tip face, with almost identical contact area, an increase of Joule heat generation in the outer contact areas by up to 27.6%. As already described in Sect.

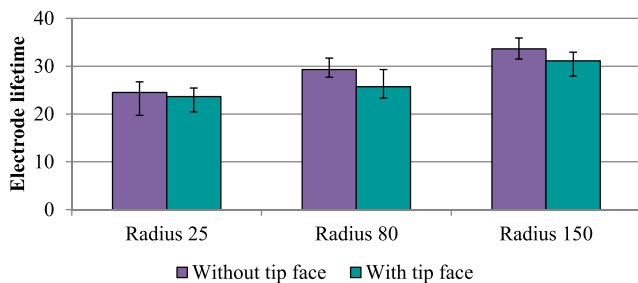


**Fig. 12** Comparison of electrode lifetime with variation of electrode cap radius and tip face

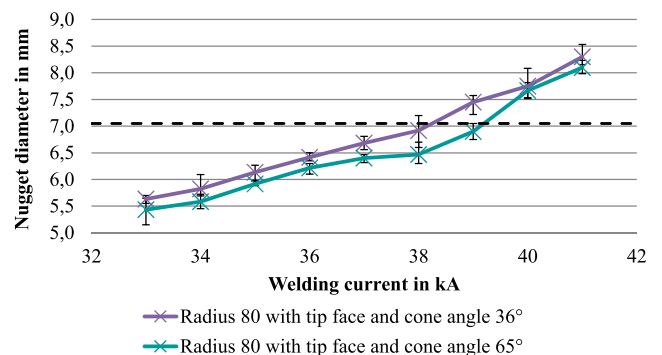


**Fig. 13** Nugget growth curve with variation of the cone angle

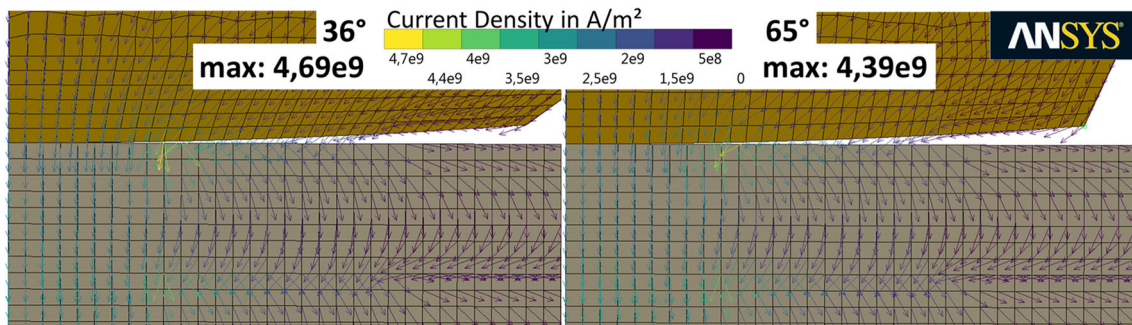


Fig. 14 Comparison of the maximum current density of electrodes with cone angle 36° (left) and 65° (right) with a current of 40 kA

4.5, this increase in reality will have an increased influence due to the microscopic contact bridge formation, as can be shown in the simulation. Furthermore, a universal cap temperature is increased by 3% over the entire welding process.

### 5.3 Influence of the electrode tip face diameter on the electrode lifetime

The determination of the influence of a tip face on the electrode lifetime shows small differences in the wear behavior. As can be seen from Fig. 12, the application of a tip face, for all radii of curvature examined, reduces the electrode life. While the lowest electrode life is expected to be achieved for the 25-radius electrodes, the largest electrode life for the 150-radius electrodes is achievable. Compared to the caps without tip face, a tapering of the tip face to 12 mm reduces the average electrode life over all radii by about 2.3 weld points. The basis for the reduction of the electrode life is the geometry-dependent change of the current density distribution in the electrode cap. The increase in the current density in the outer contacting regions that are significant for the tendency to wear (compare Fig. 11), results in additional Joule heat which enhances the diffusion processes occurring during welding. Further, factor promoting the wear is the mass loss of the electrode cap resulting from the taper, which causes a slightly deteriorated heat dissipation. The small extent of the differences in the number of positions between the caps with and without tip face is due to the choice of tip face diameter. Since this is greater than the maximum outer contact area in the experiments, no change in the indentation and associated

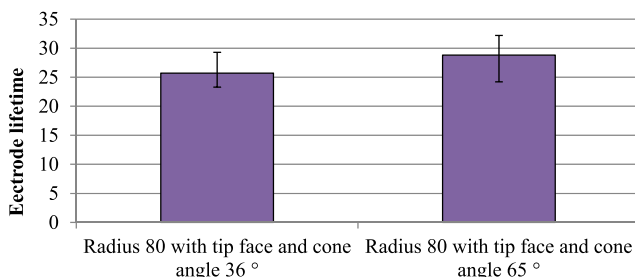


Fig. 15 Electrode lifetime with variation of the cone angle

further change in the contacting surface is observed. Based on the results in Sect. 4.5, however, it can be assumed that a combination of increased sinking into the material with the tip face dependent change in the current density will lead to an increased tendency to wear.

In summary, it should be noted that the use of electrodes with tip face is not recommended for maximizing the electrode cap level. However, if the use of a tip face is necessary due to flange-length-related restrictions on the electrode geometry, this must be carried out as far as possible than the maximum contact surface.

## 6 Investigation of the cone angle

### 6.1 Influence of the cone angle on the nugget growth

According to the literature (see [5, 7]), one significant parameter determining the heat generation when using an electrode with a tip face is the cone angle of the electrode cap taper. The growth curves of electrode caps with a cone angle of 36° and 65° shown in Fig. 13 show slight differences. As can be seen from the figure, for the electrode caps with 36° cone angle at discrete currents a higher nugget diameter is achieved. The differences in diameter with a mean difference of 3.9%, however, are relatively low. The welding current required to weld the nominal point diameter is reduced by 1 kA for the electrode caps with a 36° cone angle. The explanation for this behavior is the change in current density described by Li [5]. Due to the steeper cone angle, the current flow lines are focused earlier in the direction of the electrode and sheet contact surface and thus homogenize the global current density distribution in the electrode cap.

Figure 14 confirms the dependence of the current density on the respective cone angle on the basis of the simulated maximum current density distribution. The simulations are both done with a current of 40 kA. It can be seen that for the larger cone angle there is a more homogeneous distribution of the current density with less intense current peaks. Therefore, despite the identical contact surface, the use of flatter cone



angles results in a larger local heat quantity in the joining plane, so that formation of a welding nugget takes place even at lower current intensities.

## 6.2 Influence of the cone angle on the strength and heat generation

Due to an identical electrode radius and the same tip face diameter, no changes in the load capacity of the welded joint are to be expected. The evaluation of the simulated temperature curves and the thermographic images contradicts the simulated temperature characteristics of Li (see [5]) and shows only minor temperature differences of less than 10 °C. An indication of an analog, cone angle independent temperature generation in the cap center is also shown in Fig. 14. Although prior focusing of the current flow lines results in changes in the current density in the cap margins, the current-carrying area under the electrode cap remains constant. As a possible geometry-independent reason for the difference, the reduction in the cap mass caused by the application of the steeper cone angle by approximately 5% must additionally be taken into account. The already described change in the current density in the outer cap areas results in a local increase in Joule heat generation of up to 10%, as predicted by the simulation. Due to the comparatively small size of these areas, however, a noticeable influence on the outer cap temperature cannot be detected.

## 6.3 Influence of the cone angle on the electrode lifetime

The variation of the cone angle has an influence on the achievable electrode life. As shown in Fig. 15, a reduction in the cone angle results in a 12% reduction of electrode life. The fact that the wear for the electrode caps is increased by 36 ° angle despite reduced welding current and identical contact surfaces, can be attributed to the change in the current density maxima. This results in an increased amount of Joule heat in a locally limited area, which is particularly significant for wear, at the outer contact point. This strengthens the diffusion processes taking place there and in this way increases the electrode wear.

In summary, it can be said that when using an electrode cap with tip face the cone angle should be selected as large as possible. Through this, the current flow lines are already bended outside of the wear-critical areas, so that a homogenized current density over the total cap surface is the result.

## 7 Summary and outlook

In this article, the influence of different electrode cap geometries on the electrode life was shown experimentally and

simulatively. Starting from diameter 16 type A electrodes, the crowning of the caps was varied in the range of 25 to 300 mm. To test the tip face and the cone angle, type B electrode caps were used. The tip face was reduced to 12 mm and the investigation of the cone angles set to 65° and 36°.

Welding nugget growth curves were first created for each geometry. The electrode life examinations were carried out under constant welding nugget diameter by adjusting the welding current. The termination criterion was set with the first sticking of the sheet to the electrode. In addition to metallographic and destructive tests, thermographic images were taken.

For a better understanding of the thermal processes, a multiphysical FE model was built in ANSYS.

For the investigation of the electrode cap radius, the largest electrode life was found for caps with a radius of 150 mm. The main influence on the wear could be determined by the FE model, the homogeneity of the current density. This is mainly influenced by the prevailing contact and material resistances. The contact resistance is strongly dependent on the contact pressure between the electrode and the sheet. The material resistance is influenced by the distance of the current in the electrode cap before it flows into the plate. For the cap radius of 150 mm, an optimal balance is established between the two resistors, resulting in a homogeneous current density distribution and thus heat development.

By changing the tip face to 12 mm, the required welding current is reduced for the same size of welding nugget. This can be attributed to a changed current density and thus heat generation. In addition, the reduced levels of smaller tip faces can be attributed to this. The dependence of the electrode life on the electrode cap radius of the reduced tip face is analogous to the investigations of the type A electrodes. An influence by metallographic investigations on the electrode impression or the joining gap could not be determined.

With the same nugget diameter a reduction of the welding current by 1 kA for the change of the cone angle from 65° to 36° could be determined. This is attributed to the change in the homogeneity of the current density in the contact surface sheet-sheet. At the same time, for caps with a cone angle of 36°, increased current density was detected in the outer contact region of the electrode and the sheet. The associated increase in Joule heating leads to a reduction of the electrode life of about 12%.

An influence on the strength of the welded joint could not be determined with any geometry.

On the basis of a dynamic test, a negative influence of the joint gap for the continuous operational stability should be excluded. Furthermore, the influence of the current density change on a strongly asymmetric sheet combination as well as a transferability of the results to a three-sheet combination shall be investigated. For an improved statement of the FE-model material data from the program JMatPro should be used

in further simulations. In addition, the flow curves of the EN-AW-6016 T4 alloy have to be determined and implemented. Thus, the contact resistances can be better characterized and the deformations determined in the simulation are approximated to the reality.

## References

- Kucza JC, Butruille JR, Hank E et al (1997) Aluminum as-rolled sheet for automotive applications—effect of surface oxide on resistance spot welding and adhesive bonding behavior. In: SAE International 400 Commonwealth Drive, Warrendale, PA, United States
- DIN Deutsches Institut für Normung e.V. (2010) Resistance welding—spot welding electrode caps (DIN EN ISO 5821:2009)
- Hicken S (1997) Metallkundliche Untersuchungen zu Verschleißvorgängen an Elektroden beim Widerstandspunktschweißen von Aluminium. Techn. Hochsch., Diss.–Aachen, 1997, Als Ms. gedr. Aachener Berichte Fügetechnik, vol 97,5. Shaker, Aachen
- Hamm KJ (1989) Beitrag zur Qualitätssicherung durch Analyse des Widerstandspunktschweißprozesses beim Fügen von Aluminiumwerkstoffen. Techn. Hochsch., Diss.–Aachen, 1987. Schweißtechnische Forschungsberichte, vol 26. DVS-Verl., Düsseldorf
- Li Y, Wei Z, Li Y, Shen Q, Lin ZQ (2013) Effects of cone angle of truncated electrode on heat and mass transfer in resistance spot welding. *Int J Heat Mass Transf* 65:400–408. <https://doi.org/10.1016/j.ijheatmasstransfer.2013.06.012>
- Leuschen B (1984) Beitrag zum Tragverhalten von Aluminium- und Aluminium/Stahl-Widerstandspunktschweißverbindungen bei verschiedenartiger Beanspruchung. Fotodruck J. Mainz GmbH
- Bowers RJ, Sorensen CD, Eagar TW (1990) Electrode geometry in resistance spot welding. *Weld J* (2):45–51
- Ikeda R, Yasuda K, Hashiguchi K et al (1995) Effect of electrode configuration on electrode life in resistance spot welding of galvanized steel and aluminum alloy for car body sheets. *Proc Adv Technol Process*:144–151
- GSI SLV München (2004) Standmengenerhöhung beim Widerstandsschweißen durch Elektrodenfräsen. Schlussbericht
- Thomton M, Newton C, Keay B et al. (eds) (1996) Spot welding of aluminum sheet: a statistical approach to measuring the influence of different surfaces
- Eichhorn F, Kunsmann A (1970) Tragverhalten von Punktschweißverbindungen an 1 bis 3 mm dicken Stahlblechen bei verschiedenartiger Beanspruchung, vol 58. Deutscher Verlag für Schweißtechnik, Düsseldorf
- Osternann F (2014) Anwendungstechnologie Aluminium, 3., neu bearb. Aufl. 2014. VDI-Buch. Springer, Berlin
- Sigler DR, Carlson BE (2013) Improving aluminum resistance spot welding in automotive structures. *Weld J* (92):64–72
- Browne D, Newton C, Keay B (1996) Aluminum and steel resistance spot welding: modeling the differences. *Adv Technol Process*: 50–57
- Kunze S, Hahn O (2014) Beitrag zur Erhöhung der Prozesssicherheit beim Punktschweißen und Punktschweißkleben von Aluminiumkarosseriewerkstoffen. Univ., Diss.–Paderborn, 2013. Berichte aus dem Laboratorium für Werkstoff- und Fügetechnik, vol 100. Shaker, Herzogenrath
- Carlson BE, Sigler DR (eds) (2013) Resistance spot welding of sheet, extruded and cast aluminium using the multi-ring domed electrode
- Heilmann S, Zwahr C, Knappe A, Zschetzschke J, Lasagni AF, Füssel U (2018) Improvement of the electrical conductivity between electrode and sheet in spot welding process by direct laser interference patterning. *Adv Eng Mater* 114:1700755. <https://doi.org/10.1002/adem.201700755>
- Deutscher Verband für Schweißen und verwandte Verfahren e.V. (ed) (2013) Tagungsband 22. DVS-Sondertagung Widerstandsschweißen, Duisburg
- Florea RS, Solanki KN, Bammann DJ, Baird JC, Jordon JB, Castanier MP (2012) Resistance spot welding of 6061-T6 aluminum: failure loads and deformation. *Mater Des* 34:624–630
- DIN Deutsches Institut für Normung e.V. (2016) Resistance welding - Destructive testing of welds - Specimen dimensions and procedure for tensile shear testing resistance spot and embossed projection welds (DIN EN ISO 14273:2016–11)
- DIN Deutsches Institut für Normung e.V. (2004) Resistance welding - Procedures for determining the weldability lobe for resistance spot, projection and seam welding (DIN EN ISO 14327: 2004–06)
- GSI SLV München (2011) Entwicklung eines geeigneten Elektrodenbearbeitungsverfahrens für das Widerstandspunktschweißen von Aluminiumwerkstoffen. Schlussbericht
- Rashid M (2008) Some influences of tribology in resistance spot welding of aluminum alloys
- Gesellschaft für Schweißtechnik International mbH (2011) Entwicklung eines geeigneten Elektrodenbearbeitungsverfahrens für das Widerstandspunktschweißen von Aluminiumwerkstoffen. DVS Bericht 5160/11
- Klages E, Voigt A (2012) Visualisierung der Temperaturentwicklung der Schweißelektroden über den gesamten zeitlichen Verlauf eines Punktschweißprozesses. *Schweißen und Schneiden* 64(10)
- Heilmann S, Mathiszik C, Merx M, Müller J, Zschetzschke J, Ihlenfeldt S, Füssel U (2016) Numerical simulation strategies and test setup for resistance spot welding process with motion overlay. *Weld World* 61:35–46. <https://doi.org/10.1007/s40194-016-0403-z>
- Wan Z, Wang H-P, Wang M, Carlson BE, Sigler DR (2016) Numerical simulation of resistance spot welding of Al to zinc-coated steel with improved representation of contact interactions. *Int J Heat Mass Transf* 101:749–763. <https://doi.org/10.1016/j.ijheatmasstransfer.2016.05.023>
- Wang B, Hua L, Wang X, Song Y, Liu Y (2015) Effects of electrode tip morphology on resistance spot welding quality of DP590 dual-phase steel. *Int J Adv Manuf Technol* 83:1917–1926. <https://doi.org/10.1007/s00170-015-7703-0>
- Hamedi M, Atashparva M (2017) A review of electrical contact resistance modeling in resistance spot welding. *Weld World*. 61: 269–290. <https://doi.org/10.1007/s40194-016-0419-4>
- Sorpas 2D (2015) User Manual: Version 12
- Manladan SM, Yusoff F, Ramesh S, Fadzil M, Luo Z, Ao S (2017) A review on resistance spot welding of aluminum alloys. *Int J Adv Manuf Technol* 90(1–4):605–634. <https://doi.org/10.1007/s00170-016-9225-9>